

Original Paper

Multi-omics Reveal that c-Src Modulates the Mitochondrial Phosphotyrosine Proteome and Metabolism According to Nutrient Availability

Hala Guedouari^{a,b} Marie-Claude Savoie^{a,b} Stéphanie Jean^{a,b}
Marie-Ange Djeungoue-Petga^{a,b} Nicolas Pichaud^c Etienne Hebert-Chatelain^{a,b}

^aCanada Research Chair in Mitochondrial Signaling and Physiopathology, Moncton, NB, Canada,

^bUniversity of Moncton, Department of Biology, Moncton, NB, Canada, ^cUniversity of Moncton, Department of Chemistry and Biochemistry, Moncton, NB, Canada

Key Words

Mitochondria • c-Src kinase • Metabolism • NDUFA8 • Nutrient availability • Phosphoproteomics

Abstract

Background/Aims: Src kinase family members, including c-Src, are involved in numerous signaling pathways and have been observed inside different cellular compartments. Notably, c-Src modulates carbohydrate and fatty acid metabolism and is involved in the metabolic rewiring of cancer cells. This kinase is found within mitochondria where it targets different proteins to impact on the organelle functions and overall metabolism. Surprisingly, no global metabolic characterization of Src has been performed although c-Src knock-out mice have been available for 30 years. Considering that c-Src is sensitive to various metabolites, c-Src might represent a crucial player in metabolic adjustments induced by nutrient stress. The aim of this work was to characterize the impact of c-Src on mitochondrial activity and overall metabolism using multi-omic characterization. **Methods:** *Src*^{+/+} and *Src*^{-/-} mice were fed *ad libitum* or fasted during 24h and were then analyzed using multi-omics. **Results:** We observed that deletion of c-Src is linked to lower phosphorylation of Y412-NDUFA8, inhibition of oxygen consumption and accumulation of metabolites involved in glycolysis, TCA cycle and amino acid metabolism in mice fed *ad libitum*. Finally, metabolomics and (phosphotyrosine) proteomics are differently impacted by Src according to nutrient availability. **Conclusion:** The findings presented here highlight that c-Src reduces mitochondrial metabolism and impacts the metabolic adjustment induced by nutrient stress.

© 2020 The Author(s). Published by
Cell Physiol Biochem Press GmbH&Co. KG

Introduction

Carbohydrates are major macronutrients in energy metabolism. They are oxidized via glycolysis, tricarboxylic acid (TCA) cycle and oxidative phosphorylation (OXPHOS), which generate most of the cellular ATP. Excess carbohydrates can be converted into fatty acids and stored as triglycerides (TG) [1]. During nutrient deprivation, adjustments in metabolism allow to sustain ongoing energy requirements of cells. Notably, the liver breaks down glycogen into glucose, which is then released in the bloodstream to serve as fuel for other tissues. As fasting progresses, hepatic glycogen reserves deplete [2]. TG stored in adipose tissue are then hydrolyzed into free fatty acids (FFAs) and transported to the liver [3, 4], where they are oxidized into mitochondria to form acetyl coenzyme A (acetyl-CoA). FFA-derived acetyl-CoA can be redirected toward the production of ketone bodies such as acetoacetate and β -hydroxybutyrate (BHB) [5]. Ketone bodies represent essential alternative fuels for extrahepatic tissues during fasting [6]. The mitochondrial acetyl-CoA can also be oxidized by the TCA cycle to produce reducing equivalents (NADH and FADH₂) that will in turn allow ATP synthesis via OXPHOS. This process involves a series of five enzyme complexes embedded in the inner mitochondrial membrane. Electrons from NADH and FADH₂ are transferred through electron transport system (ETS) complexes (C) I, II, III and IV, allowing the reduction of O₂ into H₂O. Simultaneously, protons are pumped from the matrix to the intermembrane space at CI, III and IV to generate a proton gradient which is used by the ATP synthase to drive ATP synthesis [7]. Mitochondria are able to switch between different metabolic fuels such as carbohydrates and fatty acids, allowing the maintenance of metabolic homeostasis essential for cell survival during periods of nutrient stress.

Mitochondria are also biosynthetic hubs that produce a variety of signaling molecules such as reactive oxygen species (ROS) and TCA cycle intermediates [8–11]. For instance, α -ketoglutarate (α -KG) can bind and inhibit ATP synthase during glucose deprivation leading to reduced ATP content and decreased oxygen consumption in both *Caenorhabditis elegans* and mammalian cells [12]. The reduction of ATP levels activates the stress responsive metabolic regulator AMP-activated protein kinase (AMPK). In turn, AMPK inhibits the mechanistic target of rapamycin complex 1 (mTORC1) by direct phosphorylation of the tumor suppressor TSC2 or the regulatory associated protein of mTOR (known as Raptor) and lead ultimately to inhibition of cellular growth and activation of autophagy [13–15]. AMPK can also trigger mitophagy via phosphorylation of ULK1 during nutrient deprivation [16]. Simultaneously, AMPK promotes mitochondrial biogenesis via peroxisome proliferator-activated receptor γ coactivator protein -1 α (PGC-1 α) dependent transcription [17]. Overall, this highlights that nutrient sensing pathways are tightly linked to mitochondrial functions to maintain metabolic homeostasis [18, 19].

The c-Src kinase (named hereafter Src) is another important signaling effector in the control of metabolism. Src promotes glycolysis by phosphorylating both hexokinase 1 and 2 (HK1 and HK2, respectively), stimulating their catalytic activities [20]. This kinase also increases flow through the pentose phosphate pathway by activating HK when intracellular glucose is abundant [20]. Overexpression of Src increases glucose transport and glycolysis in rat and chick embryonic fibroblasts [21, 22], whereas downregulation of Src in β -cells blunts glucose-dependent ATP production [23]. In endothelial cells, the activation of glucose-6-phosphate dehydrogenase in response to vascular endothelial growth factor (VEGF) is dependent on Src-mediated tyrosine-phosphorylation [24]. It has also been shown that Src resides inside mitochondria where it targets various proteins [25–28]. Intra-mitochondrial Src inactivates pyruvate dehydrogenase (PDH), thereby attenuating the flow of glycolysis-derived pyruvate into mitochondrial oxidative metabolism in cancer cells [29]. Several components of the ETS have also been identified as targets of Src. Notably, Src phosphorylates the CI subunit NDUF10 and the CIV subunit COXII, resulting in increased activities of these complexes [27, 30]. Phosphorylation of the mitochondrial flotillin-1 by Src seems important for efficient electron transfer into complex II and the prevention of ROS production [31]. Altogether, these findings demonstrate that Src represents an important

regulator of mitochondrial metabolism. However, except for cancer cells, the role of Src in the regulation of metabolism remains scanty studied.

The overall aim of this work was to characterize the role of Src in metabolism. Src is sensitive to several metabolites, such as calcium, ATP and ROS [32–35], which are dysregulated during nutrient stress [36–39]. This strongly suggests that Src represents a potent effector of signal transduction throughout the cell to adjust metabolism during nutrient stress. Therefore, we also investigated the role of Src in the metabolic adjustment induced by fasting. To address this, we characterized hepatic mitochondrial metabolism, metabolomics and (phosphotyrosine) proteomics in *Src*^{+/+} and *Src*^{-/-} mice fed *ad libitum* or fasted for 24h. Our findings demonstrate that deletion of *Src* impacts on several metabolic pathways including glycolysis, TCA cycle, OXPHOS, as well as oxidation of amino acid and fatty acid. We also observed that Src modulates phosphorylation of the CI subunit NDUFA8, at least indirectly. Finally, this study demonstrates that Src-dependent regulation of hepatic mitochondrial metabolism differs according to nutrient availability. Globally, this work highlights the importance of Src in the maintenance of metabolic homeostasis.

Materials and Methods

Animals

All experimental procedures were approved by the Committee on Animal Care of Université de Moncton (authorization numbers 16-04, 16-05, 19-04 and 19-05). *Src*^{+/+} and *Src*^{-/-} mice (B6.129S7-*Src*^{tm1Sor}/J) were obtained from Jackson Laboratory (USA), and housed under conditions of a 12-h light/dark cycle. Experimental mice were 7 to 14 weeks old and were fed *ad libitum* with a standard rodent diet or fasted for 24h.

Mitochondrial isolation

All steps were performed at 4°C. After sacrifice, brain, liver and kidney were collected in 10 mL of isolation buffer [for brain mitochondria: 320 mM sucrose, 10 mM Tris, 1 mM EDTA, pH 7.6; for liver and kidney mitochondria: 300 mM sucrose, 5 mM Tris, 1 mM EGTA, pH 7.4] supplemented with 2 mM of the phosphatase inhibitor sodium orthovanadate (modified from [40]). Tissues were homogenized using a Teflon pestle. Brain homogenates were centrifuged at 1,500 *g* for 5 min. Supernatants were then centrifuged at 12,500 *g* for 10 min. This 2-step centrifugation cycle was repeated and the final pellet was resuspended in isolation buffer and layered on top of a discontinuous gradient of Ficoll (supplemented with 2 mM sodium orthovanadate), as described elsewhere [41]. Following centrifugation for 30 min at 100,000 *g*, mitochondrial pellets were resuspended in isolation buffer and centrifuged again for 10 min at 12,500 *g*. The resulting pelleted purified brain mitochondria were resuspended in isolation medium. Liver and kidney homogenates were centrifuged at 800 *g* for 5 min. Supernatants were then centrifuged at 8,700 *g* for 10 min. This 2-step centrifugation cycle was repeated, and the final pellet was resuspended in isolation buffer. Protein concentration was determined by Bradford assay [42].

Trypsin sensitivity assay

The sub-mitochondrial localization of Src was evaluated by treating mitochondria with 0.5% trypsin for 10 min, with or without swelling in 10 mM HEPES-KOH, 1 mM EDTA pH 7.4, with or without 1% (v/v) Triton X-100 during 10 min at 37 °C. The reaction was stopped with protease inhibitors (Bioshop, CA), and samples were processed for SDS-PAGE.

Mitochondrial Oxygen Consumption

Mitochondrial oxygen consumption assays were performed using the high-resolution respirometry system Oxygraph-2k (OROBOROS INSTRUMENTS, Austria). Mitochondrial respiration was performed with 50 µg of mitochondria in respiration buffer (75 mM mannitol, 25 mM sucrose, 100 mM KCl, 10 mM Tris, 10 mM Tris-phosphate and 50 µM EDTA [43]) at 30°C. A substrate-uncoupler-inhibitor-titration protocol [44] was used to evaluate mitochondrial capacity with different substrates and inhibitors to examine specific steps of ETS and OXPHOS: pyruvate/malate (5 mM/2 mM), glutamate/malate (10 mM/2 mM), succinate

(10 mM), 500 μ M ADP, 0.5 μ M rotenone, 2.5 μ M antimycin A. N,N,N',N'-tetramethyl-p-phenylenediamine (TMPD) and ascorbate (0.5 mM and 2 mM, respectively) were added to measure complex IV dependent respiration which was corrected for chemical background after complete inhibition by potassium cyanide (1 mM).

Enzymatic assays

All enzymatic assays were performed using a Varioskan plate reader (Flash version 2.4.5, Thermo Fisher, MA, USA) set at 37°C.

Complexes I+III. Combined activity of complex I (NADH: ubiquinone oxidoreductase) and III (coenzyme Q: cytochrome *c* – oxidoreductase) activity was determined by adding 195 μ L of assay buffer [100 mM KH_2PO_4 , pH 8.5, 0.03% Triton X-100, 2 mM idonitrotetrazolium chloride (INT), 0.85 mM NADH] to 15 μ g of mitochondria. Activity was monitored by following INT reduction at 490 nm for 4 min ($\epsilon=15.9 \text{ mL}\cdot\text{cm}^{-1}\cdot\mu\text{mol}^{-1}$).

Complex II. Mitochondria were incubated in 25 mM potassium phosphate buffer, pH 7.5 supplemented with 2 mM EDTA, 1 mg/mL BSA, 50 μ M 2, 6-dichlorophenolindophenol (DCPIP), 4 μ M rotenone, 0.2 mM ATP and 10 mM succinate for 10 min at 37°C. After addition of succinate, the baseline was read at 600 nm for at least 2 min, and the change in absorbance was then monitored for 5 min after addition of 80 μ M decylubiquinone. Malonate (10 mM) was finally added to inhibit the oxidation of succinate and the assay was run for another 5 min. Enzyme activity was calculated with $\epsilon=19.1 \text{ mL}\cdot\text{cm}^{-1}\cdot\mu\text{mol}^{-1}$ for DCPIP.

Complex IV. Complex IV (cytochrome *c* oxidase) activity was determined in isolated mitochondria, by following the oxidation of reduced cytochrome *c* at 550 nm ($\epsilon=18.5 \text{ mL}\cdot\text{cm}^{-1}\cdot\mu\text{mol}^{-1}$) for 4 min, in 50 mM potassium phosphate buffer (pH 8.0) and 80 mM reduced cytochrome *c* (freshly prepared before each experiment).

Citrate synthase. Mitochondria (15 μ g) were added in a solution containing 100 mM imidazole-HCl (pH 8.0), 0.1 mM 5, 5-dithio-bis-2-nitrobenzoic acid (DTNB), 0.2 mM oxaloacetate, and 0.1 mM acetyl-CoA. The reaction of free coenzyme A with DNTB to produce TNB was followed spectrophotometrically at 412 nm for 4 min ($\epsilon=13.6 \text{ mL}\cdot\text{cm}^{-1}\cdot\mu\text{mol}^{-1}$).

Mitochondrial H_2O_2 production

Mitochondrial H_2O_2 production was measured by the Amplex Red-horseradish peroxidase (HRP) method. Mitochondria (12.5 μ g) were resuspended in respiration buffer containing 5 mM glutamate with 2.5 mM malate for brain mitochondria or 2.5 mM pyruvate with 2.5 mM malate for liver and kidney mitochondria, 10 mM succinate and 500 μ M ADP. Fluorescence was followed using a Varioskan plate reader (Flash version 2.4.5, Thermo Fisher, MA, USA) with excitation wavelength set at 560 nm and emission wavelength set at 587 nm. The increased fluorescence over time was converted to the rate of H_2O_2 production using a standard curve with known H_2O_2 concentrations. All assays were performed at 37°C, in black 96-well plates.

Western blot analysis

Samples were analyzed by western blot analysis using conventional methods. Samples were diluted in SDS-PAGE sample buffer [62.5 mM Tris pH 6.8, 10 % (v/v) glycerol, 2 % (w/v) sodium dodecylsulfate (SDS), 0.5 % Bromophenol blue, 2.5 % (v/v) β -mercapto-ethanol] and boiled at 95°C during 5 min. Samples were then separated using 7, 10 or 12 % SDS-polyacrylamide mini-gel at 300 V during 30 min. Proteins were blotted to polyvinylidene difluoride membranes and detected using specific antibodies against Src (Cell signaling; 2108S), phosphoY416-Src (Cell signaling; 6943S), phosphotyrosine (Cell signaling; 9411S), SDHA (Abcam; ab14715), SMAC (Cell signaling; 15108S), TOM20 (Santa Cruz; sc-17764), SOD2 (Cell signaling; 13194S), ATP5a (Abcam; ab14748), NDUF9a (Abcam; ab14713), cytochrome *c* (Abcam; ab133504). The blots were visualized by chemiluminescence and band intensities were quantified by densitometric analysis using Image Lab software (BioRad).

Blood glucose monitoring

Blood samples were collected from mice after cervical dislocation without anesthesia. Glucose levels were measured using a glucometer ACCU-CHECK (Roche Diagnostics, Japan). All measurements were performed following the manufacturer's instructions.

Liver glycogen content measurement

Liver samples were snap-frozen in liquid nitrogen and stored at -80°C . The glycogen content was measured using a fluorometric Glycogen Assay Kit (Ref. 700480, Cayman Chemical, USA). All measurements were performed by following the manufacturer's instructions.

Metabolomic analysis by GC-MS

GC-MS experiments were performed at the metabolomics core facility at the Rosalind and Morris Goodman Cancer center (McGill University, Canada). Liver samples were pulverized on dry ice and were weighed in the range of $10\text{ mg} \pm 1\text{ mg}$. 1 mL volume of 80 % (v/v) methanol/water and three pre-chilled 2.8 mm ceramic beads were added to each sample. Samples were subjected to three rounds of bead beating for 2 min at 30 Hz using a Qiagen Tissue Lyser (Eppendorf, Canada). Samples were then centrifuged for 10 min at 15,000 rpm (4°C). Supernatants were transferred to new pre-chilled tubes containing 1 μL of 800 ng/ μL $^2\text{H}_{27}$ -Myristic in pyridine. Samples were then dried by vacuum centrifugation operating at a sample temperature of -4°C .

After drying, samples were subjected to a two-step derivatization for GC-MS analysis. Following GC/MS scan and single ion monitoring (SIM) data acquisition, samples were diluted using 30 % methoxyamine hydrochloride and 70 % N-tert-Butyldimethylsilyl-N-methyltrifluoroacetamide 1:14 and data were acquired in scan mode. An Agilent 5975C GC-MS equipped with a DB-5MS+DG (30 m x 250 μm x 0.25 μm) capillary column (Agilent J&W, Santa Clara, CA, USA) was used for all GC-MS experiments, and data were collected by electron impact set at 70 eV both in scan (50-1000 m/z) and single ion monitoring (SIM) modes. Sample data were acquired in scan mode (50-1000 m/z) or in SIM with a 5 ms dwell time where the M-57 [$\text{M}^{++}\text{-C}_4\text{H}_9$] $^+$ fragment was used for relative quantitation (area under the curve) in both modes of data acquisition. The spectra and retention times of all metabolites reported were confirmed by methoxylamine-tert-butyldimethylsilylated authentic standards. Area under the curve was normalized to tissue weight.

(Phosphotyrosine) proteomic analyses by LC-MS/MS

Sample preparation. Protein digestion, peptide labeling, and mass spectrometry analyses were performed by the proteomics platform of the CHU de Quebec research center (Canada). Liver mitochondrial lysates suspended in 50 mM ammonium bicarbonate (ABC) / 0.5 % Deoxycholate (DOC) were vortexed and sonicated on ice. Extracts were centrifuged at 13,000 rpm during 15 min. The obtained supernatant was precipitated in acetone and centrifuged again. The resulting pellet was resuspended in 50 mM ABC with 1.0 % DOC. Then, 400 μg proteins were reduced, alkylated, digested with trypsin (ratio 1:50) and incubated overnight at 37°C . Samples were acidified with 1% formic acid and desalted using an HLB column (Waters, USA).

Phosphotyrosine enrichment. Phosphotyrosine peptides were enriched using PTMScan Phospho-Tyrosine antibody (P-Tyr-1000; Cell Signaling; 8803). Peptides were incubated with beads for 2 h at 4°C with gentle agitation. To remove non-specifically bound peptides, beads were washed with ice-cold Immunoaffinity Purification buffer (IAP) twice and with ice-cold water three times. Elution of phosphopeptides was carried out at room temperature using 0.15 % trifluoroacetic acid (TFA).

Mass spectrometry. Samples (global or phosphotyrosine peptides) were analyzed using an Orbitrap Fusion mass spectrometer (Thermo Fisher Scientific) connected to a Dionex UltiMate 3000 nanoRSLC chromatography system (Thermo Fisher Scientific, CA, USA). Peptides were eluted on a Pepmap Acclaim 50 cm x 75 μm internal diameter separation column (ThermoFisher) with a linear gradient from 4-32 % acetonitrile in 0.1% formic acid during 90 min (phosphopeptide) or 240 min (global), at 300 nL/min. Mass spectra were acquired using a data-dependent acquisition mode using Thermo XCalibur software (v 4.1.50).

Database searching and Label-Free Quantification. Spectra were searched against the Uniprot Ref Mus musculus database (61364 entries) using the Andromeda module of MaxQuant software v. 1.6.0.16 [45]. Trypsin/P enzyme parameter was selected with two possible missed cleavages. Carbamidomethylation of cysteines was set as fixed modification while methionine oxidation and phosphorylation of serine, threonine, and tyrosine were set as variable modifications (for the phosphopeptides). Mass search tolerance was 5 ppm and 0.5 Da for MS and MS/MS respectively. For protein validation, a maximum False Discovery Rate of 1 % at peptide and protein level was used based on a target/decoy search. MaxQuant was also used for Label-Free Quantification. RStudio (v 1.1.383) was used for data processing. A normalization step was performed using the median of intensities of each condition. Missing values were replaced by a noise value

corresponding to 1% percentile of the normalized value for each condition. A peptide was considered as quantifiable only if at least three intensity values in one of the two samples were present or not more than one value missing per condition. For the global analysis, at least 2 peptides per protein were required for quantification.

Statistical analyses

Student's T test and two-way ANOVA followed by Tukey's post-hoc test, were performed using GraphPad Prism 8 (v 8.2.1), as appropriate. For metabolomic and (phosphotyrosine) proteomic analyses, partial least squares discriminant analyses (PLS-DA) were performed using MetaboAnalyst 3.0 [46, 47]. Normalization (by log transformation) was performed in order to minimize possible differences in concentration between samples. All data were mean centered and scaled to unit variance. PLS-DA identified the metabolites driving the separation and/or clustering among experimental groups by ascribing a variable importance of projection score (VIP). Significance was set at $p < 0.05$.

Results

Deletion of *Src* impairs mitochondrial metabolism in brain, liver and kidney

We first evaluated the levels of Src in brain, liver, and kidney isolated mitochondria. Results showed that Src levels are significantly higher in brain than in liver and kidney (Fig. 1a and Supplementary Fig. S1a – for all supplemental material see www.cellphysiolbiochem.com). Trypsin sensitivity assays confirmed that mitochondrial Src mostly resides inside the organelle (Fig. 1b) as previously shown [27, 48]. These results also suggest that Src is also localized in the mitochondrial matrix considering it is resistant to trypsin upon swelling of liver mitochondria.

The functional impact of Src was then evaluated by measuring the oxygen consumption of brain, liver and kidney enriched-mitochondrial fractions isolated from *Src*^{+/+} and *Src*^{-/-} mice. Deletion of *Src* significantly decreased oxygen consumption of brain, liver and kidney mitochondria in the presence of (i) glutamate with malate (for brain mitochondria), or pyruvate with malate (for liver and kidney mitochondria), (ii) with the addition of ADP, and (iii) with further addition of succinate (Fig. 1c-e). No difference in respiration was observed when inhibitors of CI and III (rotenone and antimycin A, respectively) were added, or when maximum capacity of CIV was measured in presence of TMPD and ascorbate (Fig. 1c-e). These results indicate that Src is required to maintain mitochondrial respiration. We then measured the enzymatic activity of CI+III, II and IV. Deletion of *Src* significantly decreased the activity of CI+III and II in brain, liver, and kidney mitochondria (Fig. 1f and g). Deletion of *Src* also decreased CIV activity in brain mitochondria, had no effect in liver mitochondria and increased CIV activity in kidney mitochondria (Fig. 1h). Citrate synthase (CS) activity was decreased in liver mitochondria but unchanged in brain and kidney mitochondria upon deletion of *Src* (Fig. 1i). These findings indicate that Src has tissue-specific impact on CIV and CS.

Immunoblotting assays showed that levels of the mitochondrial proteins ATP5a, SDHa, NDUF9A, SOD2 and TOM20 are similar in brain, liver, and kidney mitochondria isolated from *Src*^{+/+} and *Src*^{-/-} mice (Fig. 1j and Supplementary Fig. S1b). These findings demonstrate that the decreased mitochondrial respiration observed in *Src*^{-/-} mice is not due to decreased mitochondrial content. Mitochondrial H₂O₂ production was not altered by deletion of *Src* (Fig. 1k). Overall, these results suggest that Src targets ETS components to regulate mitochondrial metabolism, likely via tyrosine-phosphorylation.

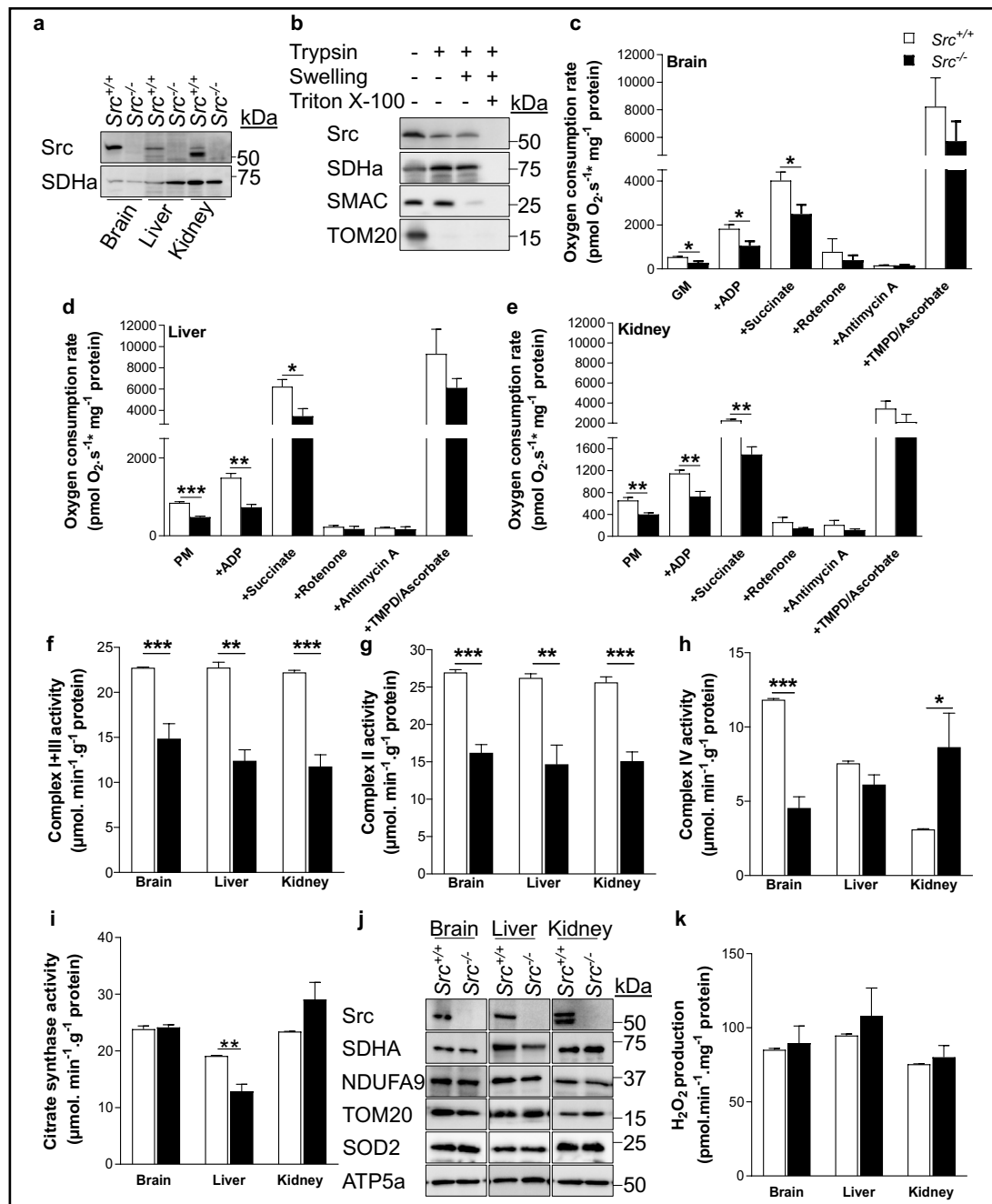


Fig. 1. Deletion of Src impairs mitochondrial metabolism in brain, liver and kidney. (a) Representative immunoblots (n=4) of Src and SDHa (as loading control) in brain, liver and kidney mitochondria isolated from Src^{+/+} and Src^{-/-} mice (fed ad libitum). See Fig. S1a for quantification. (b) Representative immunoblots (n=3) of Src, the inner mitochondrial membrane protein SDHa, the mitochondrial intermembrane space protein SMAC and the outer membrane mitochondrial protein TOM20 in liver mitochondria treated as indicated, showing that Src is mostly located inside mitochondria. (c-e) Oxygen consumption rates of brain (c), liver (d) and kidney (e) mitochondria isolated from Src^{+/+} and Src^{-/-} mice (fed ad libitum) in the presence of different substrates and inhibitors, as indicated (n=4). GM: Glutamate/Malate, PM: Pyruvate/Malate. (f-i) Enzymatic activities of complexes I+III (f), II (g) and IV (h), and citrate synthase (i) in brain, liver and kidney mitochondria isolated from Src^{+/+} and Src^{-/-} mice fed ad libitum. (j) Representative immunoblots (n=4) of Src, SDHa, NDUFA9, TOM20, SOD2 and ATP5a in brain, liver and kidney mitochondria isolated from Src^{+/+} and Src^{-/-} mice fed ad libitum. See Fig. S1b for quantification. (k) H₂O₂ production by brain, liver and kidney mitochondria isolated from Src^{+/+} and Src^{-/-} mice fed ad libitum (n=4). Data are presented as mean ± s.e.m. *p<0.05, **p<0.01, ***p<0.001 determined by Student's T test.

Effect of Src on hepatic mitochondrial activity according to nutrient availability

The liver plays a crucial role in maintaining energy balance and metabolic homeostasis during starvation. Src activity is sensitive to metabolites such as ATP and ROS [33, 34, 49, 50], which are affected during nutrient stress. Therefore, we sought to determine the role of Src in the adjustment of hepatic metabolism during nutrient stress. To address this, we analyzed *Src*^{+/+} and *Src*^{-/-} mice either fed *ad libitum* or fasted during 24h. Fasting decreased blood glucose and hepatic glycogen in both genotypes (Fig. 2a and b). We then examined different respiration rates of *Src*^{+/+} and *Src*^{-/-} liver enriched-mitochondrial fractions using (i) pyruvate, malate and ADP, to follow respiration via CI+III+IV, (ii) pyruvate, malate, succinate and ADP to follow CI+II+III+IV-dependent respiration, and (iii) TMPD and ascorbate to follow CIV-dependent respiration after inhibition of complexes I and III (Fig. 2c-e). Deletion of *Src* significantly decreased CI+III+IV and CI+II+III+IV-dependent respiration in mice fed *ad libitum* but not in fasted mice (Fig. 2c and d). Respiration rates were also lower in fasted *Src*^{+/+} and *Src*^{-/-} mice compared to *Src*^{+/+} control mice (Fig. 2c and d). CIV-dependent respiration rate was not statistically different among experimental groups (Fig. 2e). Similar to CI+III+IV and CI+II+III+IV respiration rates, enzymatic activity of CI+III was significantly lower in *Src*^{-/-} than in *Src*^{+/+} liver mitochondria from fed mice, whereas fasting reduced CI+III activity only in *Src*^{+/+} liver mitochondria (Fig. 2f). Liver CII activity was decreased by deletion of *Src* in mice fed *ad libitum* (Fig. 2g). Surprisingly, fasting increased liver CII activity in both *Src*^{+/+} and *Src*^{-/-} mice (Fig. 2g), suggesting CII does not play a major role in the observed fasting-dependent inhibition of respiration rates. Liver CIV catalytic activity was only significantly decreased by fasting in *Src*^{+/+} mice (Fig. 2h). CS activity was lower upon deletion of *Src* in mice fed *ad libitum*, whereas this reduction was not observed in fasted mice (Fig. 2i). Similar to CII, this finding suggests that CS is not involved in Src-dependent regulation of respiration during fasting. Immunoblottings of SDHa, ATP5a, NDUFA9, SOD2, TOM20, and cyt *c* showed that mitochondrial protein levels are similar among groups (Fig. 2j and Supplementary Fig. S1c). No change in mitochondrial H₂O₂ production was observed after fasting (Fig. 2k). Our findings suggest that the observed Src-dependent alteration of mitochondrial oxygen consumption in liver is mediated by post-translational modification (i.e., tyrosine-phosphorylation) of CI and/or CIII and depends on nutrient availability.

Effect of Src on hepatic metabolomics according to nutrient availability

To further characterize the role of Src in metabolism, we analyzed *Src*^{+/+} and *Src*^{-/-} mice fed *ad libitum* and fasted for 24h using untargeted GC-MS metabolomics. We identified 41 metabolites involved in various pathways related to metabolism of glucose, fatty acids, amino acids, ketone bodies and nucleotides (Fig. 3 and Supplementary Fig. S2). Metabolomes were analyzed using multivariate PLS-DA [46, 47] to evaluate how they were affected by Src during fasting (Fig. 3a). The two main PLS components, PC1 and PC2, explained 16.3% and 28.1% of the total variance, respectively. Interestingly, two-dimensional score plots showed that the metabolomes of *Src*^{+/+} and *Src*^{-/-} fasted mice cluster with *Src*^{+/+} mice fed *ad libitum* (Fig. 3a), further confirming that the effect of Src on metabolism depends on nutrient availability. Variable importance of projection (VIP) scores identified 12 metabolites significantly driving (i.e., metabolites with VIP score > 1) the specific metabolomic signature among experimental groups (Fig. 3b). Among these key metabolites, TCA cycle intermediates succinate, fumarate, and malate were all significantly increased after deletion of *Src* in mice fed *ad libitum* whereas fumarate and malate were decreased by fasting only in *Src*^{-/-} mice (Fig. 3c). Glycolytic intermediates DHAP and 3-phosphoglycerate were significantly decreased upon fasting only in *Src*^{-/-} mice (Fig. 3d), whereas pyruvate was significantly decreased by deletion of *Src* in fasted mice (Fig. 3d). Levels of amino acids aspartate, glutamate, glutamine and histidine were higher in *Src*^{-/-} mice fed *ad libitum*, whereas their levels decreased upon fasting only in *Src*^{-/-} mice (Fig. 3e). Levels of taurine were significantly increased by fasting in both *Src*^{+/+} and *Src*^{-/-} mice (Fig. 3e). Similarly, levels of the ketone body 3-hydroxybutyrate was significantly increased for both *Src*^{+/+} and *Src*^{-/-} mice in response to fasting (Fig. 3f). Several other metabolites involved in different metabolic pathways did not vary among experimental

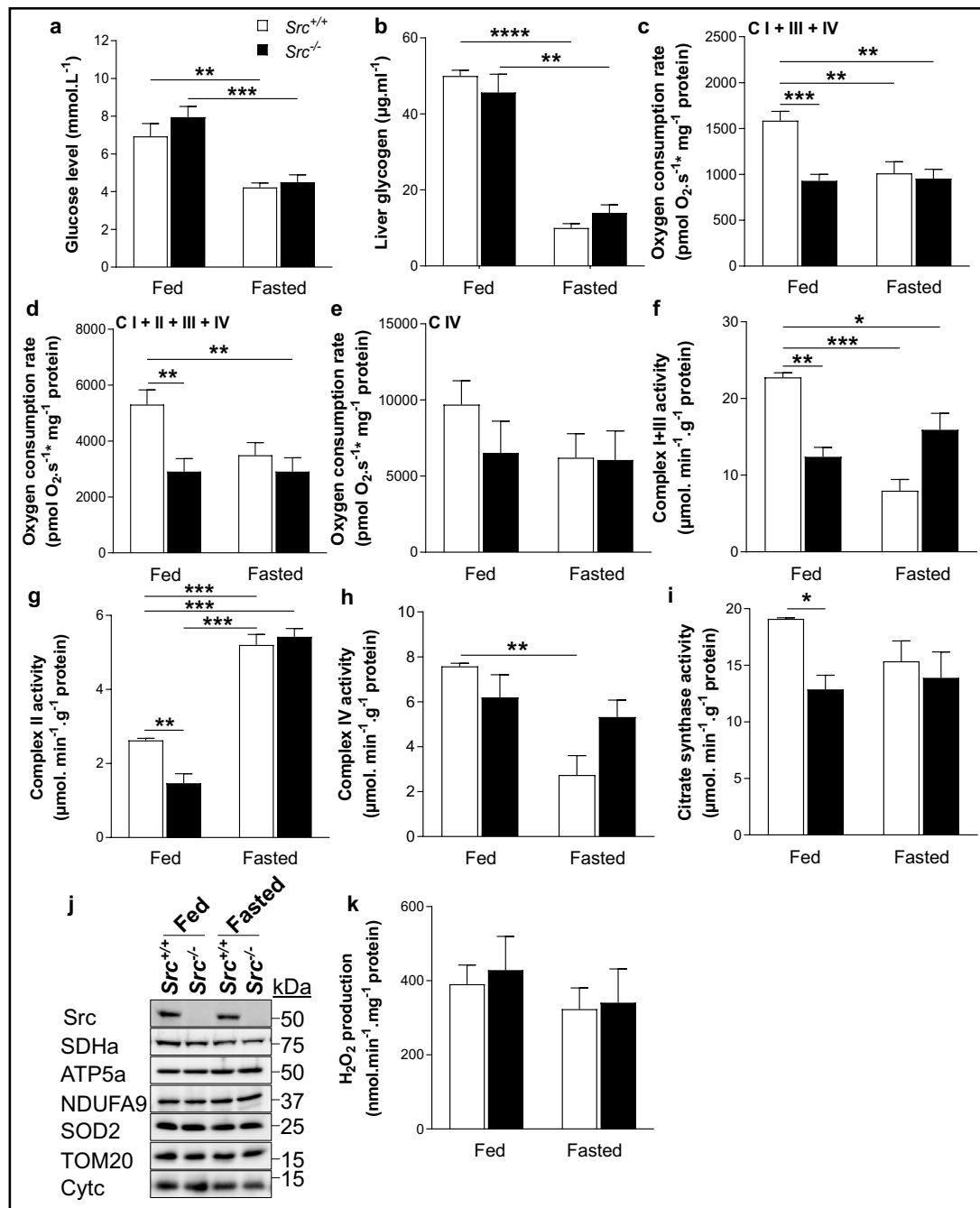


Fig. 2. Modulation of mitochondrial metabolism by Src according to nutrient availability. (a, b) Levels of blood glucose (a) and liver glycogen (b) in fed and fasted Src^{+/+} and Src^{-/-} mice (n=3). (c-e) Oxygen consumption rates of liver mitochondria obtained from fed and fasted Src^{+/+} and Src^{-/-} mice (n=7) in presence of specific substrates and inhibitors to evaluate complex CI+III+IV-dependent respiration (c), CI+II+III+IV-dependent respiration (d), and CIV-dependent respiration (e). (f-i) Enzymatic activities of complexes I+III (f), complex II (g), complex IV (h) and citrate synthase (i) in liver of fed and fasted Src^{+/+} and Src^{-/-} mice (n=4). (j) Representative immunoblots (n=4) of Src, SDHa, ATP5a, NDUFA9, SOD2, TOM20 and Cytc in liver of fed and fasted Src^{+/+} and Src^{-/-} mice. See Fig. S1c for quantification. (k) H₂O₂ production by liver mitochondria isolated from fed and fasted Src^{+/+} and Src^{-/-} mice (n=5). Data are presented as mean ± s.e.m. *p<0.05, **p<0.01, ***p<0.001, ****p<0.0001 determined by a two-way ANOVA followed by post-hoc Tukey's test.

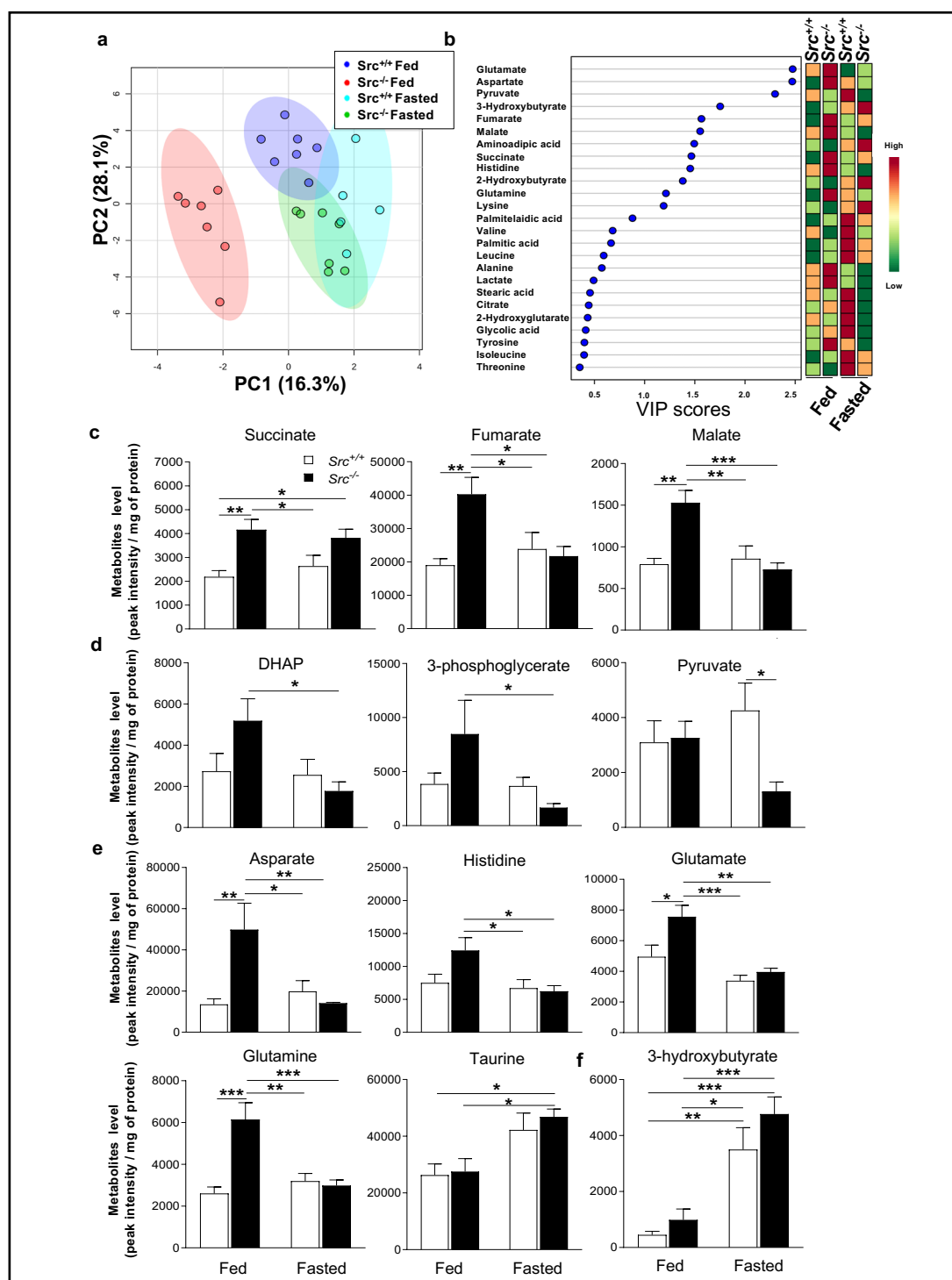


Fig. 3. Modulation of metabolomics by Src according to nutrient availability. (a) PLS-DA score plots of metabolites in fed or fasted Src^{+/+} and Src^{-/-} mice. Ellipses represent 95 % confidence intervals for each individual group on PLS-DA plots with the variance proportion represented by principal components 1 and 2 (PC1 & PC2, respectively). (b) Variable importance of projection (VIP) scores of PLS-DA, which identify the key metabolites driving the metabolomic signature for fed and fasted Src^{+/+} and Src^{-/-} mice. (c-f) Quantitative analysis of intermediates of TCA cycle (c) and glycolysis/neoglucogenesis (d), amino acids (e) and ketone bodies (f) identified as drivers of the metabolomic signature of Src^{+/+} and Src^{-/-} mice fed ad libitum or fasted. See also Fig. S2 for metabolites not significantly different among experimental groups. Data are presented as mean ± s.e.m. (n = 7). *p < 0.05, **p < 0.01, ***p < 0.001 determined by a two-way ANOVA followed by post-hoc Tukey's test.

groups (Supplementary Fig. S2). Globally, these results suggest that ETS defects induced by deletion of *Src* in fed mice result in accumulation of intermediates of TCA cycle and amino acid metabolism. However, this accumulation is no longer observed in fasted mice, as the levels of metabolites were mostly similar between *Src*^{+/+} and *Src*^{-/-} mice.

Effect of Src on the hepatic proteome according to nutrient availability

The mitochondrial proteome of liver enriched-mitochondrial fractions derived from fed and fasted *Src*^{+/+} and *Src*^{-/-} mice was then characterized by nanoLC-MS/MS. Among the identified proteins (Supplementary Table S1), 612 are mitochondrial proteins (Supplementary Table S2). Considering that the mitochondrial proteome includes approximately 1,000 proteins [51] (as compared to 14,000 proteins in the total liver proteome), we obtained a ~5-fold enrichment of mitochondrial proteins in our liver mitochondria-enriched fractions (see also Supplementary Fig. S3a). PLS-DA of all the detected proteins showed that the hepatic proteomic signatures of fed and fasted *Src*^{+/+} mice cluster together whereas fed and fasted *Src*^{-/-} mice have different proteomic signatures (Fig. 4a). Procedures to isolate mitochondria are designed to yield enriched fractions of functional mitochondria. However, they are not designed to enrich proteins from all the subcellular compartments equally and likely lead to an over- and/or under-representation of proteins from other specific compartments. We thus repeated PLS-DA only on the detected mitochondrial proteins to avoid such bias. The mitochondrial proteomic signature among experimental groups was similar to the signature observed when all the proteins identified in our mitochondria-enriched fractions were considered (Fig. 4a and b), confirming that the variance observed in our proteomic analysis is mostly explained by changes in mitochondrial proteins. Among the identified mitochondrial proteins, 83 proteins had significant impact (VIP score > 1) on the mitochondrial proteomic signature among the different groups (Fig. 4c, Table 1 and Supplementary Table S3). Interestingly, most of these proteins are involved in metabolism of fatty acid, pyruvate and amino acid. Among these 83 proteins, two-way ANOVA revealed significant genotype×diet interaction only for glycine amidinotransferase (GATM) and acyl-coenzyme A thioesterase 9 (ACOT9) (Fig. 4d and Supplementary Fig. S3b), confirming that Src-dependent modulation of metabolism does not involve major change in mitochondrial mass. Deletion of *Src* significantly increased the levels of GATM and ACOT9 in mice fed *ad libitum* but not in fasted mice (Fig. 4d), corroborating that the impact of Src differs between fed and fasted mice.

Effect of Src on the hepatic phosphotyrosine proteome according to nutrient availability

To understand the role of Src-mediated signaling on hepatic metabolism, we first examined the level and activity of Src in liver enriched-mitochondrial fractions. The results showed that fasting induces activation of Src (Fig. 5a and b, Supplementary Fig. S4a). To identify the mitochondrial proteins potentially targeted by Src, we quantitatively analyzed tyrosine-phosphorylated proteins among liver enriched-mitochondrial fractions derived from fed and fasted *Src*^{+/+} and *Src*^{-/-} mice using immuno-enrichment of phosphotyrosine peptides and nanoLC-MS/MS. We detected 701 tyrosine-phosphorylated peptides (Supplementary Table S4), among which 79 correspond to mitochondrial proteins (Supplementary Table S5 and Fig S4b). PLS-DA using all the identified phosphopeptides showed different phosphotyrosine proteomic signatures for each individual experimental group (Fig. 5b). Again, to avoid bias due to the presence of over- or under-represented phosphopeptides from extra-mitochondrial compartments, we repeated PLS-DA using only the 79 mitochondrial phosphopeptides, and obtained similar phosphotyrosine proteomic signatures (Fig. 5c). Among the mitochondrial phosphotyrosine peptides, 13 had VIP score > 1 (Fig. 5d and Table 2) and were considered crucial to the phosphotyrosine proteomic signature among the four experimental groups. These phosphotyrosine peptides correspond to proteins with various molecular functions, including OXPHOS as well as metabolism of fatty acid and amino acid. Two-way ANOVA revealed significant genotype×diet interaction for one phosphotyrosine peptide corresponding to NDUFA8, a nuclear-encoded subunit of CI (Fig. 5e and Fig S4c). We also observed a significant decrease of phosphorylated Y142-NDUFA8 upon deletion of *Src*

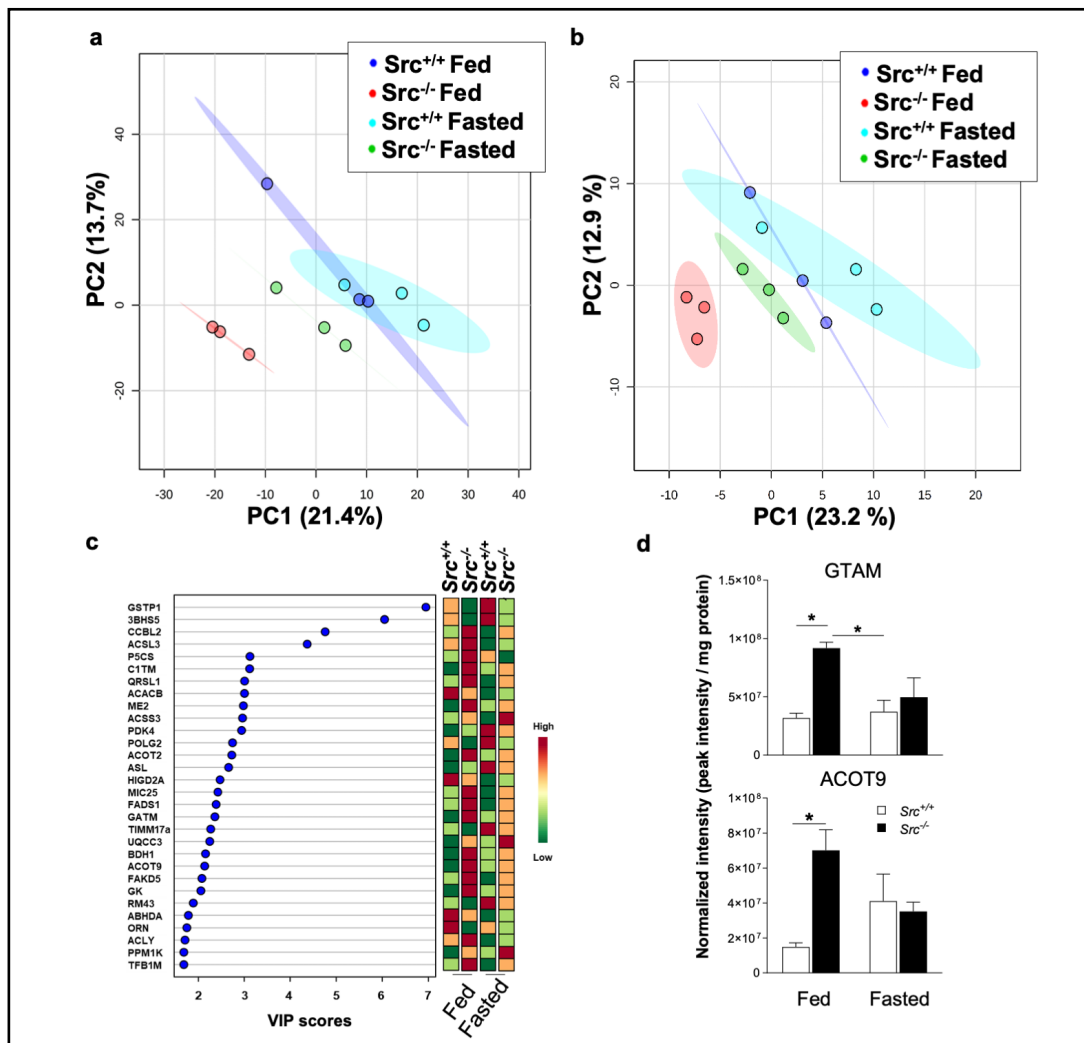


Fig. 4. The impact of Src on liver proteome according to nutrient availability. (a, b) PLS-DA plots showing different proteomic signatures for Src^{+/+} and Src^{-/-} mice fed ad libitum or fasted considering all proteins (a) or only mitochondrial proteins (b) detected by nanoLC-MS/MS. Ellipses represent 95 % confidence intervals for each individual group on PLS-DA plots with the variance proportion represented by principal components 1 and 2 (PC1 & PC2, respectively). (c) Variable importance of projection (VIP) scores of PLS-DA, identifying the key proteins driving the proteomic signatures for fed and fasted Src^{+/+} and Src^{-/-} mice. (d) Quantitative analysis of proteins (with VIP score ≥ 2) driving the proteomic signature of Src^{+/+} and Src^{-/-} mice fed ad libitum or fasted. See also Fig. S3 for key proteins that are not significantly different among experimental groups. Data are mean \pm SEM (n = 3). *p<0.05 determined by a two-way ANOVA followed by post-hoc Tukey's test.

in mice fed *ad libitum* (Fig. 5e). Phosphorylation of Y142-NDUFA8 was however increased upon deletion of *Src* in fasted mice, suggesting that this residue might be targeted by other kinases. *In silico* analyses using the NetPhos 3.1 online tool (<http://www.cbs.dtu.dk/index.php>) predicted a probability of 0.456 that Src directly phosphorylates Y142-NDUFA8. Similar results were obtained using the GPS online tool (prediction score: 2.708; <http://gps.biocuckoo.cn>). Overall, phosphoproteomic analyses support the hypothesis that Src impacts on hepatic metabolism in a nutrient availability dependent manner.

Table 1. Mitochondrial proteins significantly driving the mitochondrial proteomic signature among Src+/+ and Src-/- mice fed ad libitum or 24h-fasted. Only proteins with VIP score > 2 are presented. See Supplementary Table S3 for all proteins with VIP score > 1

Accession	Gene name	Protein name
P19157	Gstp1	Glutathione S-transferase P 1
Q61694	Hsd3b5	NADPH-dependent 3-keto-steroid reductase
Q71RI9	Ccbl2	Kynurenine--oxoglutarate transaminase 3
Q9CZW4	Acsl3	Long-chain-fatty-acid--CoA ligase 3
Q9Z110	Aldh18a1	Delta-1-pyrroline-5-carboxylate synthase
Q3V3R1	Mthfd11	Monofunctional C1-tetrahydrofolate synthase
Q9CZN8	Qrs1	Glutamyl-tRNA(Gln) amidotransferase subunit A
E9Q4Z2	Acacb	Acetyl-CoA carboxylase 2
Q99KE1	Me2	NAD-dependent malic enzyme
Q14DH7	Acss3	Acyl-CoA synthetase short-chain family member 3
O70571	Pdk4	[Pyruvate dehydrogenase (acetyl-transferring)] kinase isozyme 4
Q9QZM2	Polg2	DNA polymerase subunit gamma-2
Q9QYR9	Acot2	Acyl-coenzyme A thioesterase 2
Q91YI0	Asl	Argininosuccinate lyase
Q9CQJ1	Higd2a	HIG1 domain family member 2A
E9Q4M4	Mic25	MICOS complex subunit
Q920L1	Fads1	Acyl-CoA (8-3)-desaturase
Q9D964	Gatm	Glycine amidinotransferase
Q9Z0V8	Timm17a	Mitochondrial import inner membrane translocase subunit Tim17-A
Q8K2T4	Uqcc3	Ubiquinol-cytochrome-c reductase complex assembly factor 3
Q80XN0	Bdh1	D-beta-hydroxybutyrate dehydrogenase
Q9R0X4	Acot9	Acyl-coenzyme A thioesterase 9
Q7TMV3	Fakd5	FAST kinase domain-containing protein 5
Q64516	Gk;Gyk	Glycerol kinase

Table 2. Phosphorylation sites among mitochondrial proteins significantly driving the phosphotyrosine proteomic signature in liver mitochondria derived from Src+/+ and Src-/- mice fed ad libitum or 24h-fasted. Only proteins with VIP score > 1 are presented

Accession	Gene name	Protein name	Phospho-site
Q9DCJ5	Ndufa8	NADH dehydrogenase 1 alpha subcomplex subunit 8	Y142
P56395	Cyb5a	Cytochrome b-5	Y136
O08599	Stxbp1	Syntaxin-binding protein 1	Y473
O08756	Hsd17b10	Short chain L-3-hydroxyacyl-CoA dehydrogenase	Y277
P16460	Ass1	Argininosuccinate synthase	Y87
P05202	Got2	Aspartate aminotransferase	Y96
P14234	Fgr	Tyrosine-protein kinase Fgr	Y400
P49710	Hcls1	Hematopoietic lineage cell-specific protein	Y103
Q9CQ54	Ndufc2	NADH dehydrogenase 1 subunit C2	Y109
Q9WV60	Gsk3b	Glycogen synthase kinase-3 beta	Y216
Q8VCF0	Mavs	Mitochondrial antiviral-signaling protein	Y216
Q9EQ20	Aldh6a1	Methylmalonate-semialdehyde dehydrogenase	Y268
Q9CRD0	Ociad1	O CIA domain-containing protein 1	Y212

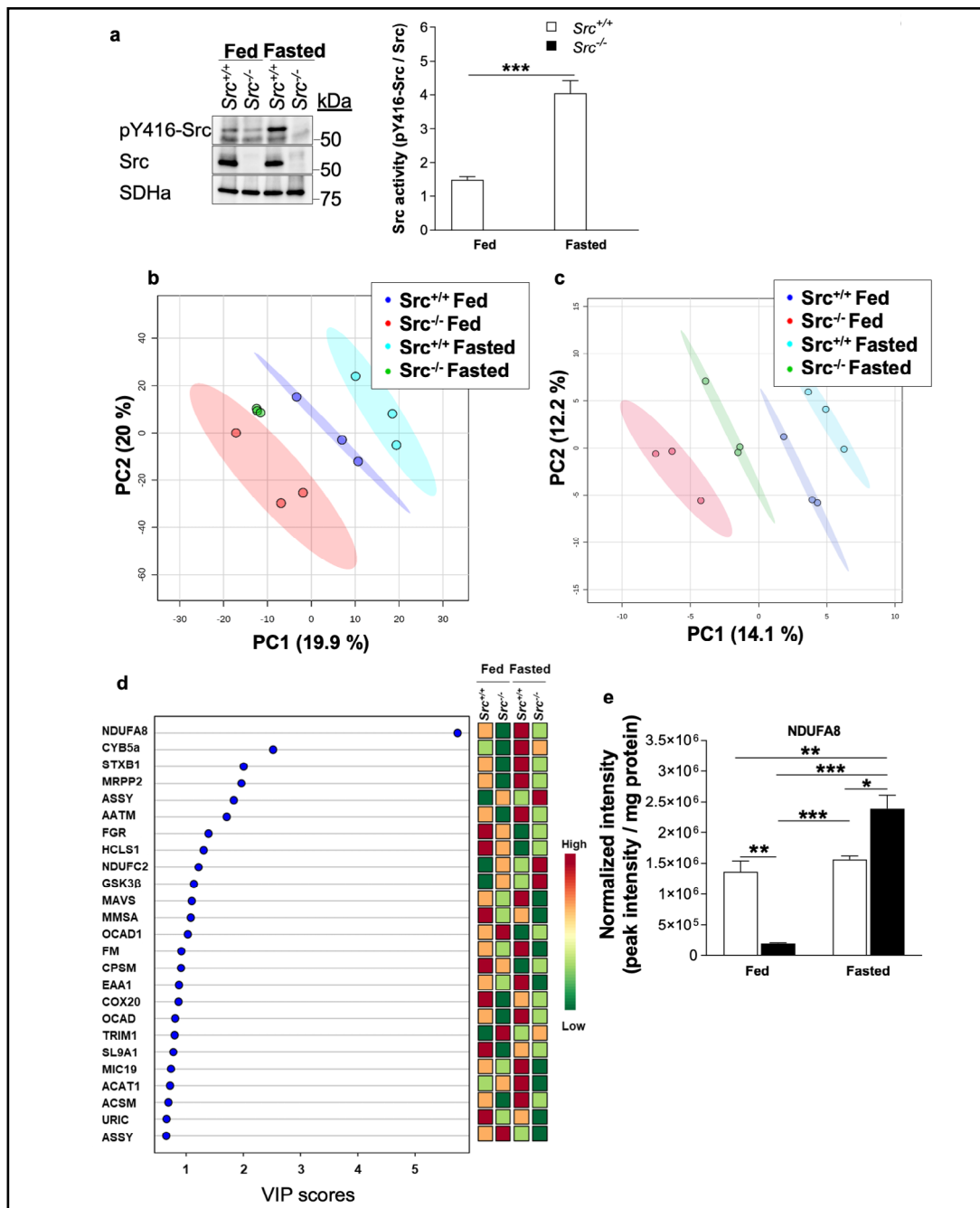


Fig. 5. The impact of Src on mitochondrial phosphotyrosine proteomics according to nutrient availability. (a) Top. Representative immunoblots (n=4) of pY416-Src, total Src and SDHa in liver mitochondria isolated from Src^{+/+} and Src^{-/-} mice fed ad libitum or fasted during 24h. Note that the faint pY416-Src signal in Src^{-/-} mice is likely due to other Src kinases present in liver mitochondria. Bottom. Quantification of Src activity (labeling of pY416-Src normalized to Src labeling), indicating that Src activity is higher upon fasting. (b, c) PLS-DA plots showing phosphotyrosine proteomic signatures of Src^{+/+} and Src^{-/-} mice fed ad libitum or fasted when all phosphotyrosine peptides (b) or only mitochondrial phosphotyrosine peptides (c) detected by nanoLC-MS/MS were considered. (d) Variable importance of projection (VIP) scores of PLS-DA which identify the key proteins driving the phosphotyrosine proteomic signatures of fed and fasted Src^{+/+} and Src^{-/-} mice. (e) Quantitative analysis of phosphopeptides driving the phosphotyrosine proteomic signature of Src^{+/+} and Src^{-/-} mice fed ad libitum or fasted. See also Fig. S5 for key phosphotyrosine proteins not significantly different among experimental groups. Data are mean ± s.e.m. (n = 3). *p<0.05, **p<0.01, ***p<0.001 determined by a two-way ANOVA followed by post-hoc Tukey's test.

Discussion

Src is involved in multiple signaling pathways maintaining cellular homeostasis during metabolic stress. Notably, Src directly targets mitochondrial proteins to impact on mitochondrial functions [29, 30, 49]. Although metabolic stress can lead to dysregulation of Src activity and mitochondrial metabolism [36–39], the impact of Src on metabolic homeostasis during challenging nutrient conditions remains poorly understood. The aim of our study was thus to characterize the role of Src in metabolism. Our findings suggest that deletion of *Src* inhibits hepatic OXPHOS. Using omics, we also showed that deletion of *Src* alters TCA cycle, amino acid and fatty acid metabolism as well as phosphorylation of Y142-NDUFA8 (Fig. 6). Our findings highlight the role of Src as a central player in mitochondrial metabolism and its impacts on the metabolic adjustment to nutrient stress.

This work confirms that Src can target OXPHOS components since it is present inside mitochondria, as previously described [26, 27]. Intra-mitochondrial Src was previously shown to be associated to IMM using immunogold labeling [26, 27]. Here, we showed that mitochondrial Src is also resistant to degradation by trypsin after swelling of isolated organelles. This finding thus suggests that Src is also localized in matrix, and that it could have other targets than only IMM proteins facing the IMS.

We identified 13 phosphotyrosine residues that were linked to the overall phosphotyrosine proteomic signature of *Src*^{+/+} and *Src*^{-/-} mice fed or fasted, including Y142-NDUFA8, Y136-CYB5A and Y109-NDUFC2. The only protein with lower tyrosine-phosphorylation in *Src*^{-/-} mice is the CI subunit NDUFA8. Phosphorylation of Y142-NDUFA8 was ≈7-fold lower upon deletion of *Src* in mice fed *ad libitum*. NDUFA8 subunit is part of the proton pumping P-module of CI [52]. This subunit is located at the proximal end of the membrane arm and faces the intermembrane space, which is consistent with our findings and previous observations showing that Src is located within mitochondria [53]. NDUFA8 is considered as an accessory subunit essential for the proper assembly of the quinone binding Q module [54]. Interestingly, the alteration of Y142-NDUFA8 phosphorylation induced by the anaesthetic propofol is associated with reduced levels of several CI subunits in HT22 cells [55]. It is therefore possible that phosphorylation status of Y142-NDUFA8 would impact assembly and stability of CI in *Src*^{-/-} mice. Our data however suggest that phosphorylation status of Y142-NDUFA8 is not sufficient to explain functional changes of mitochondrial metabolism since levels of phosphorylated Y142-NDUFA8 peptides do not match respiration rates among *Src*^{+/+} and *Src*^{-/-} mice fed *ad libitum* or fasted during 24h. Also, our findings do not allow to conclude that Src phosphorylates NDUFA8 directly or indirectly. First, *in silico* analyses revealed significant probability that Src targets directly Y142-NDUFA8. Phosphorylation of this protein however increased in *Src*^{-/-} mice upon fasting, suggesting that other kinases could target this residue. It is thus possible that Y142-NDUFA8 is mainly phosphorylated by Src when mice are fed *ad libitum* and targeted by other kinases in fasted *Src*^{-/-} mice. Future studies should examine whether Src can directly phosphorylate this residue. Src could also target (directly or not) other proteins inside hepatic mitochondria for which phosphotyrosine residue(s) could have been lost during the experimental procedure. Notably, enzymatic activities of CII and CS were decreased in liver mitochondria after deletion of *Src* although these proteins were not detected in our phosphoproteomic characterization. Several previously identified targets of mitochondrial Src, such as NDUFB10 and COXII [27, 30], were also not detected in the present study. It is possible that such phosphorylation events appear in a cell type-specific manner. For instance, over-expression of Src specifically in mitochondria did not alter phosphorylation of COXII in breast cancer cells MDA-MB-231 [56].

Hundreds of phosphorylation sites have been previously identified among mitochondrial proteins using various approaches and tissues [57]. Phosphotyrosines usually represent less than 1-10% of phosphorylation events in global proteomic studies: 35 phosphotyrosine residues among 594 phosphorylation sites were recently reported in rat liver mitochondria [58] whereas 16 phosphotyrosines among 155 phosphorylation sites were reported in human

skeletal mitochondria [59]. Here, we identified 79 tyrosine-phosphorylated mitochondrial proteins upon immuno-enrichment of phosphotyrosine. These proteins are located in different mitochondrial compartments and involved in several processes, such as OXPHOS (including the CIV subunit NDUFA4 and the CIV assembly factor COX20), metabolism of fatty and amino acids (including acyl-coenzyme A synthetase 1 and aspartate aminotransferase) as well as mitochondrial dynamics (including MICOS complex subunit 19 and prohibitin). Interestingly, similar tyrosine-phosphorylation of ANT1 and ANT2 was previously observed [60]. It will be important to compare levels of dephosphorylated and phosphorylated peptides to examine the functional impact of these individual phosphorylation sites in future studies. Various tyrosine-phosphorylated mitochondrial proteins previously identified were however not observed in the present study. These discrepancies suggest that tyrosine-phosphorylation is a fine-tuned process rather than a nonspecific event. For instance, rat liver mitochondria are enriched in phosphoproteins involved in amino acid and fatty acid metabolism, whereas heart and skeletal muscle mitochondria are enriched in phosphoproteins involved in TCA cycle and OXPHOS [58]. Also, a significant fraction of phosphotyrosines reported in the literature were observed in cancer tissue and cells (see www.phosphosite.org), in which several tyrosine kinases, including Src, are over-activated [61]. It is therefore possible that phosphotyrosine levels are lower in non-cancer tissue. Our technical procedures could have nevertheless removed several phosphosites. For instance, freezing-thawing between isolation of mitochondrial fractions and phosphoproteomics could have resulted in loss of phosphorylation sites.

Although they have been available for decades, no metabolic characterization of *Src*^{-/-} mice has been performed. Our findings demonstrate that deletion of *Src* induces major metabolic shifts in liver (Fig. 6). In various types of tumors, overexpression or overactivation of this kinase stimulates glucose uptake [62], hexokinase activity and production of lactate [20], whereas it inhibits pyruvate dehydrogenase [29] and OXPHOS [56]. Here, *Src*^{-/-} mice showed accumulation of the TCA cycle intermediates succinate, fumarate and malate despite similar glycogen and blood glucose availability. It is thus possible that inhibition of ETS complexes resulted in accumulation of metabolites upstream of ETS. Several glycolytic and other TCA cycle metabolites were however not increased in *Src*^{-/-} mice. Fatty acid oxidation and catabolism of amino acid could have also been increased to compensate the inhibition of ETS induced by deletion of *Src*. For instance, we observed increased levels of GATM and accumulation of the amino acids aspartate, glutamate and glutamine in *Src*^{-/-} mice fed *ad libitum*. Src is necessary for amino acid-dependent mTORC1 activation and its translocation to lysosomes [63], a central mechanism for the induction of autophagy. The accumulation of amino acids in *Src*^{-/-} mice could thus be due to lower activity of mTORC1 and autophagic machinery. Deletion of *Src* also increased the level of ACOT9 which converts fatty acyl-CoA thioesters into free fatty acids and CoA [64]. Mice null for the Src kinase family member Fyn display increased fatty acid oxidation [65], suggesting that Src could have a similar effect. ACOT9 can also hydrolyze short-chain methyl branched acyl-CoAs such as propionyl-CoA and methyl nonanoyl-CoA, that are metabolic end products of β -oxidation and amino acid metabolism [64, 66]. Here, the accumulation of succinate, fumarate and malate observed in *Src*^{-/-} mice could thus result from higher production of succinyl-CoA by increased levels of ACOT9. We therefore suggest that Src is central to maintain equilibrium among metabolism of carbohydrate, fatty acid and amino acid.

Multivariate analysis of metabolomics and (phosphotyrosine) proteomics demonstrated specific phenotypic signatures for control and *Src*^{-/-} mice, indicating that Src is important for the hepatic metabolic adjustment induced by nutrient stress. Src activity was increased in liver mitochondria-enriched fractions upon fasting, likely to allow adjustment of metabolism to nutrient deprivation. Activation of Src kinases is a common phenomenon observed in various types of metabolic stress. For instance, ATP levels are maintained by upregulated fatty acid oxidation in triple negative breast cancer cells, leading to auto-activation of Src and higher metastasis potential [67]. Similarly, Fyn activity is increased in macrophage from mice fed a high-fat diet [68], suggesting that the higher activation of Src observed in liver

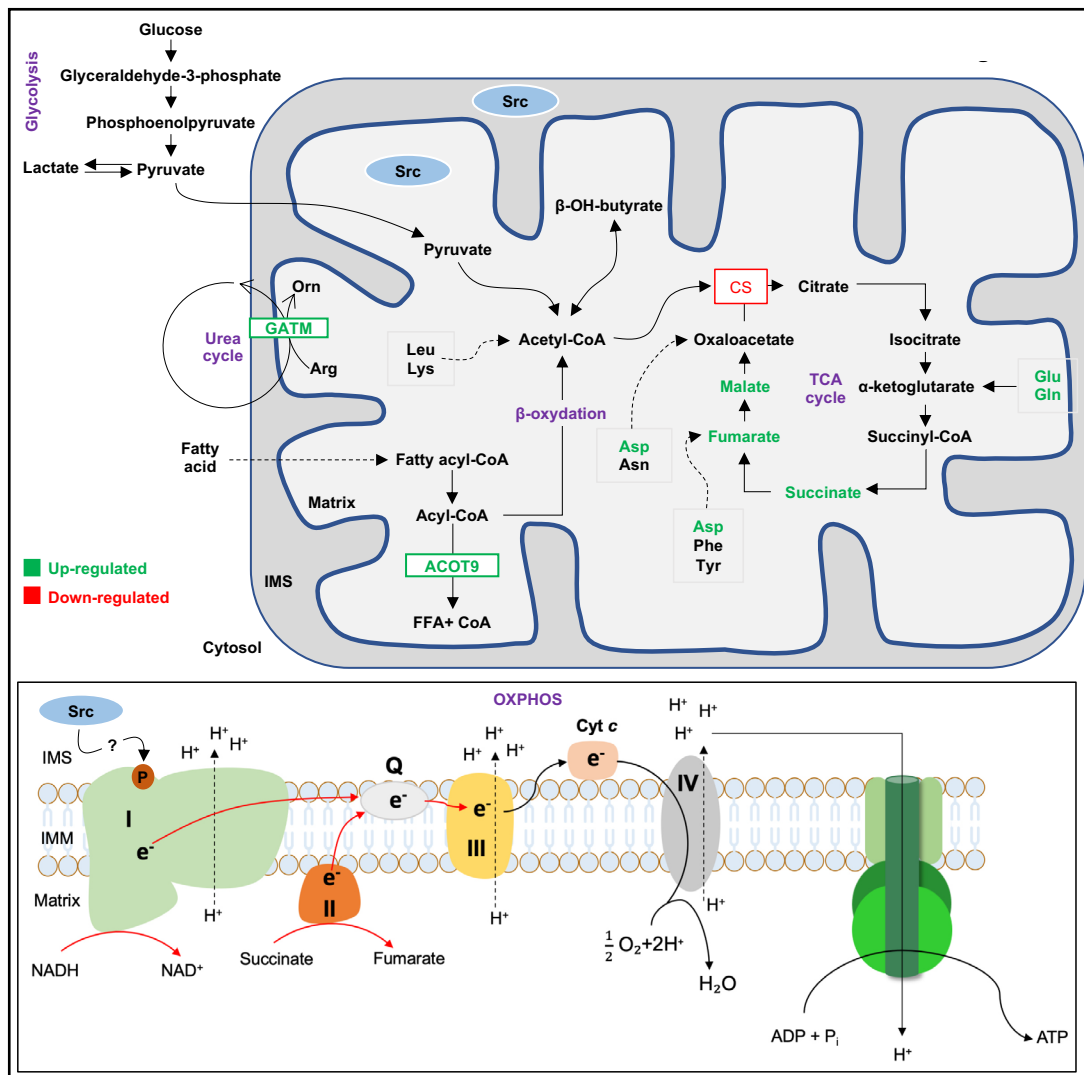


Fig. 6. Deletion of Src induces shifts in hepatic metabolism. Representation of metabolic alterations observed in liver of Src^{-/-} mice. Major metabolic pathways are indicated (in purple): glycolysis, urea cycle, β -oxidation, tricarboxylic (TCA) cycle and oxidative phosphorylation (OXPHOS). Oxidation of amino acids are also indicated. Previous works suggested that Src is present in IMS whereas our findings indicate that Src is also localized in the matrix. Deletion of Src increased levels of proteins GTAM (glycine amidinotransferase) and Acyl-CoA thioesterase 9 (ACOT9), amino acids aspartate (Asp), glutamate (Glu), glutamine (Gln) and of TCA cycle intermediates malate, fumarate and succinate (indicated in green) in liver of mice fed ad libitum. These changes were associated with lower activities of citrate synthase (CS), and of electron transport system complexes I, II and III (indicated by red arrows) in liver of Src^{-/-} mice fed ad libitum. Phosphotyrosine proteomic analyses showed lower levels of phosphorylated NDUFA8 in liver of Src^{-/-} mice fed ad libitum, suggesting that Src target (directly or indirectly) this CI subunit. Arg: Arginine; Asn: Asparagine; Asp: Aspartate; Cyt c: Cytochrome c; e⁻: electron; Gln: glutamine; Glu: glutamate; FFA: Free Fatty Acid; IMM: Inner Mitochondrial Membrane; IMS: Intermembrane Space; Leu: Leucine; Lys: Lysine; Orn: Ornithine; Phe: Phenylalanine; Q: Ubiquinone; Tyr: Tyrosine.

mitochondria-enriched fractions from Src^{+/+} fasted mice could have been induced by higher fatty acid oxidation. In this study, pyruvate level was decreased in Src^{-/-} fasted mice despite similar glycogen and blood glucose availability. PDH activity is inhibited by fasting in skeletal muscle [69] and by Src kinase [29, 69], suggesting that glycolysis is not the main pathway fueling oxidative metabolism in Src^{-/-} fasted mice.

Conclusion

In conclusion, our work demonstrates that Src has a significant impact on metabolism in multiple tissues, including brain, kidney and liver. Deletion of *Src* induces inhibition of mitochondrial respiration and alters intermediates and proteins involved in metabolism of carbohydrates, amino acid and fatty acid. The present study also reports several tyrosine-phosphorylated mitochondrial proteins involved in various functions, ranging from OXPHOS, metabolism of fatty acid or amino acid, to mitochondrial dynamics. Future experiments will be necessary to examine how Src modulates oxidation of amino acid and fatty acid, test whether Src can directly target Y142-NDUFA8 and evaluate the functional impacts of the reported phosphotyrosine sites including Y142-NDUFA8.

Acknowledgements

We are grateful to Patrick Roy for animal care. GC-MS experiments were performed at the metabolomics core facility at the Rosalind and Morris Goodman Cancer center (McGill University, Canada). LC-MS/MS was performed by the Proteomics Platform of the CHU de Quebec research center, Quebec city, Quebec, Canada.

Author Contributions

HG, NP and EHC designed the study. HG, MCS, SJ and MADJ performed experiments. HG, MCS, NP and EHC analyzed data. HG, NP and EHC wrote and edited the manuscript. All authors approved the final version of the manuscript.

Funding

This work was funded by the Canadian Cancer Society (2015-317342), Natural Sciences and Engineering Research Council of Canada (NSERC, RGPIN-2015-05880), Canadian Health Research Institute (CIHR, 388808), Canada Research Chair program, New Brunswick Health Research Foundation, New Brunswick Innovation Foundation and Université de Moncton. NP is funded by NSERC (RGPIN-2017-05100).

Disclosure Statement

The authors have no conflicts of interest to declare.

References

- 1 Teusink B, Voshol PJ, Dahlmans VEH, Rensen PCN, Pijl H, Romijn JA, et al.: Contribution of fatty acids released from lipolysis of plasma triglycerides to total plasma fatty acid flux and tissue-specific fatty acid uptake. *Diabetes* 2003;52:614–620.
- 2 Crabtree B: Energy metabolism in animals and man. *Biochem Educ* 1990;18:218.
- 3 Tobey JA: The Biology of Human Starvation. *Am J Public Health Nations Health* 1951;41:236–237.
- 4 Hashimoto T, Cook WS, Qi C, Yeldandi AV, Reddy JK, Rao MS: Defect in Peroxisome Proliferator-activated Receptor α -inducible Fatty Acid Oxidation Determines the Severity of Hepatic Steatosis in Response to Fasting. *J Biol Chem* 2000;275:28918–28928.
- 5 Heijboer AC, Donga E, Voshol PJ, Dang ZC, Havekes LM, Romijn JA, et al.: Sixteen hours of fasting differentially affects hepatic and muscle insulin sensitivity in mice. *J Lipid Res* 2005;46:582–588.
- 6 Owen OE: Ketone bodies as a fuel for the brain during starvation. *Biochem Mol Biol Educ* 2005;33:246–251.
- 7 Mitchell P: Coupling of Phosphorylation to Electron and Hydrogen Transfer by a Chemi-Osmotic type of Mechanism. *Nature* 1961;191:144–148.

- 8 Mehta MM, Weinberg SE, Chandel NS: Mitochondrial control of immunity: beyond ATP. *Nat Rev Immunol* 2017;17:608–620.
- 9 Schieber M, Chandel NS: ROS Function in Redox Signaling and Oxidative Stress. *Curr Biol* 2014;24:R453–R462.
- 10 Sullivan LB, Gui DY, Vander Heiden MG: Altered metabolite levels in cancer: implications for tumour biology and cancer therapy. *Nat Rev Cancer* 2016;16:680–693.
- 11 Sciacovelli M, Frezza C: Oncometabolites: Unconventional triggers of oncogenic signalling cascades. *Free Radic Biol Med* 2016;100:175–181.
- 12 Chin RM, Fu X, Pai MY, Vergnes L, Hwang H, Deng G, et al.: The metabolite α -ketoglutarate extends lifespan by inhibiting ATP synthase and TOR. *Nature* 2014;510:397–401.
- 13 Gwinn DM, Shackelford DB, Egan DF, Mihaylova MM, Mery A, Vasquez DS, et al.: AMPK phosphorylation of raptor mediates a metabolic checkpoint. *Mol Cell* 2008;30:214–226.
- 14 Polak P, Hall MN: mTOR and the control of whole body metabolism. *Curr Opin Cell Biol* 2009;21:209–218.
- 15 Mihaylova MM, Shaw RJ: The AMP-activated protein kinase (AMPK) signaling pathway coordinates cell growth, autophagy, & metabolism. *Nat Cell Biol* 2011;13:1016–1023.
- 16 Egan DF, Shackelford DB, Mihaylova MM, Gelino SR, Kohnz RA, Mair W, et al.: Phosphorylation of ULK1 (hATG1) by AMP-activated protein kinase connects energy sensing to mitophagy. *Science* 2011;331:456–461.
- 17 Cunningham JT, Rodgers JT, Arlow DH, Vazquez F, Mootha VK, Puigserver P: mTOR controls mitochondrial oxidative function through a YY1-PGC-1 α transcriptional complex. *Nature* 2007;450:736–740.
- 18 Efeyan A, Comb WC, Sabatini DM: Nutrient-sensing mechanisms and pathways. *Nature* 2015;517:302–310.
- 19 Scarpulla RC: Nucleus-encoded regulators of mitochondrial function: integration of respiratory chain expression, nutrient sensing and metabolic stress. *Biochim Biophys Acta* 2012;1819:1088–1097.
- 20 Zhang J, Wang S, Jiang B, Huang L, Ji Z, Li X, et al.: c-Src phosphorylation and activation of hexokinase promotes tumorigenesis and metastasis. *Nat Commun* 2017;8:13732.
- 21 Flier J, Mueckler M, Usher P, Lodish H: Elevated levels of glucose transport and transporter messenger RNA are induced by ras or src oncogenes. *Science* 1987;235:1492–1495.
- 22 Bosca L, Mojena M, Ghysdael J, Rousseau GG, Hue L: Expression of the v-src or v-fps oncogene increases fructose 2,6-bisphosphate in chick-embryo fibroblasts. Novel mechanism for the stimulation of glycolysis by retroviruses. *Biochem J* 1986;236:595–599.
- 23 Sato H, Nagashima K, Ogura M, Sato Y, Tahara Y, Ogura K, et al.: Src regulates insulin secretion and glucose metabolism by influencing subcellular localization of glucokinase in pancreatic β -cells. *J Diabetes Investig* 2016;7:171–178.
- 24 Pan S, World CJ, Kovacs CJ, Berk BC: Glucose 6-Phosphate Dehydrogenase Is Regulated Through c-Src-Mediated Tyrosine Phosphorylation in Endothelial Cells. *Arterioscler Thromb Vasc Biol* 2009;29:895–901.
- 25 Livigni A, Scorziello A, Agnese S, Adornetto A, Carlucci A, Garbi C, et al.: Mitochondrial AKAP121 Links cAMP and src Signaling to Oxidative Metabolism. *Mol Biol Cell* 2006;17:263–271.
- 26 Tibaldi E, Brunati AM, Massimino ML, Stringaro A, Colone M, Agostinelli E, et al.: Src-Tyrosine kinases are major agents in mitochondrial tyrosine phosphorylation. *J Cell Biochem* 2008;104:840–849.
- 27 Miyazaki T, Neff L, Tanaka S, Horne WC, Baron R: Regulation of cytochrome c oxidase activity by c-Src in osteoclasts. *J Cell Biol* 2003;160:709–718.
- 28 Arachiche A, Augereau O, Decossas M, Pertuiset C, Gontier E, Letellier T, et al.: Localization of PTP-1B, SHP-2, and Src exclusively in rat brain mitochondria and functional consequences. *J Biol Chem* 2008;283:24406–24411.
- 29 Jin Y, Cai Q, Shenoy AK, Lim S, Zhang Y, Charles S, et al.: Src drives the Warburg effect and therapy resistance by inactivating pyruvate dehydrogenase through tyrosine-289 phosphorylation. *Oncotarget* 2016;7:25113–25124.
- 30 Hebert-Chatelain E, Jose C, Gutierrez Cortes N, Dupuy JW, Rocher C, Dachary-Prigent J, et al.: Preservation of NADH ubiquinone-oxidoreductase activity by Src kinase-mediated phosphorylation of NDUFB10. *Biochim Biophys Acta* 2012;1817:718–725.
- 31 Ogura M, Yamaki J, Homma MK, Homma Y: Phosphorylation of flotillin-1 by mitochondrial c-Src is required to prevent the production of reactive oxygen species. *FEBS Lett* 2014;588:2837–2843.
- 32 Sorensen M, Sanz A, Gómez J, Pamplona R, Portero-Otín M, Gredilla R, et al.: Effects of fasting on oxidative stress in rat liver mitochondria. *Free Radic Res* 2006;40:339–347.

- 33 Guderley H, Lapointe D, Bédard M, Dutil JD: Metabolic priorities during starvation: enzyme sparing in liver and white muscle of Atlantic cod, *Gadus morhua* L. *Comp Biochem Physiol A Mol Integr Physiol* 2003;135:347–356.
- 34 Salin K, Villasevil EM, Anderson GJ, Auer SK, Selman C, Hartley RC, et al.: Decreased mitochondrial metabolic requirements in fasting animals carry an oxidative cost. *Funct Ecol* 2018;32:2149–2157.
- 35 Bourguignon A, Rameau A, Toullec G, Romestaing C, Roussel D: Increased mitochondrial energy efficiency in skeletal muscle after long-term fasting: its relevance to animal performance. *J Exp Biol* 2017;220:2445–2451.
- 36 Zhang J, Xing D, Gao X: Low-power laser irradiation activates Src tyrosine kinase through reactive oxygen species-mediated signaling pathway. *J Cell Physiol* 2008;217:518–528.
- 37 Mehdi MZ, Pandey NR, Pandey SK, Srivastava AK: H2O2-Induced Phosphorylation of ERK1/2 and PKB Requires Tyrosine Kinase Activity of Insulin Receptor and c-Src. *Antioxid Redox Signal* 2005;7:1014–1020.
- 38 Lakshmi S, Joshi PG: Activation of Src/kinase/phospholipase c/mitogen-activated protein kinase and induction of neurite expression by ATP, independent of nerve growth factor. *Neuroscience* 2006;141:179–189.
- 39 Weigand KM, Swarts HGP, Fedosova NU, Russel FGM, Koenderink JB: Na,K-ATPase activity modulates Src activation: A role for ATP/ADP ratio. *Biochim Biophys Acta* 2012;1818:1269–1273.
- 40 Helmy N, Prip-Buus C, Vons C, Lenoir V, Abou-Hamdan A, Guedouari-Bounihi H, et al.: Oxidation of hydrogen sulfide by human liver mitochondria. *Nitric Oxide* 2014;41:105–112.
- 41 Clark JB, Nicklas WJ: The Metabolism of Rat Brain Mitochondria. Preparation and characterization. *J Biol Chem* 1970;245:4724–4731.
- 42 Hammond JB, Kruger NJ: The Bradford method for protein quantitation. *Methods Mol Biol* 1988;3:25–32.
- 43 Melser S, Pagano Zottola AC, Serrat R, Puente N, Grandes P, Marsicano G, et al.: Functional Analysis of Mitochondrial CB1 Cannabinoid Receptors (mtCB1) in the Brain. *Meth Enzymol* 2017;593:143–174.
- 44 Christiansen LB, Dela F, Koch J, Yokota T: Tissue-specific and substrate-specific mitochondrial bioenergetics in feline cardiac and skeletal muscles. *J Vet Med Sci* 2015;77:669–675.
- 45 Cox J, Mann M: MaxQuant enables high peptide identification rates, individualized p.p.b.-range mass accuracies and proteome-wide protein quantification. *Nat Biotechnol* 2008;26:1367–1372.
- 46 Chong J, Wishart DS, Xia J: Using MetaboAnalyst 4.0 for Comprehensive and Integrative Metabolomics Data Analysis. *Curr Protoc Bioinformatics* 2019;68:e86.
- 47 Chong J, Yamamoto M, Xia J: MetaboAnalystR 2.0: From Raw Spectra to Biological Insights. *Metabolites* 2019;9:57.
- 48 Miyazaki T, Tanaka S, Sanjay A, Baron R: The role of c-Src kinase in the regulation of osteoclast function. *Mod Rheumatol* 2006;16:68.
- 49 Ogura M, Yamaki J, Homma MK, Homma Y: Mitochondrial c-Src regulates cell survival through phosphorylation of respiratory chain components. *Biochem J* 2012;447:281–289.
- 50 Sorensen M, Sanz A, Gómez J, Pamplona R, Portero-Otín M, Gredilla R, et al.: Effects of fasting on oxidative stress in rat liver mitochondria. *Free Radic Res* 2006;40:339–347.
- 51 Pagliarini DJ, Calvo SE, Chang B, Sheth SA, Vafai SB, Ong SE, et al: A mitochondrial protein compendium elucidates complex I disease biology. *Cell* 2008;134:112–123.
- 52 Sánchez-Caballero L, Guerrero-Castillo S, Nijtmans L: Unraveling the complexity of mitochondrial complex I assembly: A dynamic process. *Biochim Biophys Acta* 2016;1857:980–990.
- 53 Salvi M, Brunati AM, Bordin L, La Rocca N, Clari G, Toninello A: Characterization and location of Src-dependent tyrosine phosphorylation in rat brain mitochondria. *Biochim Biophys Acta* 2002;1589:181–195.
- 54 Szklarczyk R, Wanschers BFJ, Nabuurs SB, Nouws J, Nijtmans LG, Huynen MA: NDUFB7 and NDUFA8 are located at the intermembrane surface of complex I. *FEBS Lett* 2011;585:737–743.
- 55 Zhang H, Ye J, Shi Z, Bu C, Bao F: Quantitative analyses of the global proteome and phosphoproteome reveal the different impacts of propofol and dexmedetomidine on HT22 cells. *Sci Rep* 2017;7:46455.
- 56 Djeungoue-Petga MA, Lurette O, Jean S, Hamel-Côté G, Martín-Jiménez R, Bou M, et al.: Intramitochondrial Src kinase links mitochondrial dysfunctions and aggressiveness of breast cancer cells. *Cell Death Dis* 2019;10:940.
- 57 Kruse R, Højlund K: Mitochondrial phosphoproteomics of mammalian tissues. *Mitochondrion* 2017;33:45–57.

- 58 Bak S, León IR, Jensen ON, Højlund K: Tissue specific phosphorylation of mitochondrial proteins isolated from rat liver, heart muscle, and skeletal muscle. *J Proteome Res* 2013;12:4327–4339.
- 59 Zhao X, León IR, Bak S, Mogensen M, Wrzesinski K, Højlund K, et al.: Phosphoproteome analysis of functional mitochondria isolated from resting human muscle reveals extensive phosphorylation of inner membrane protein complexes and enzymes. *Mol Cell Proteomics* 2011;10:M110.000299.
- 60 Lewandrowski U, Sickmann A, Cesaro L, Brunati AM, Toninello A, Salvi M: Identification of new tyrosine phosphorylated proteins in rat brain mitochondria. *FEBS Lett* 2008;582:1104–1110.
- 61 Yeatman TJ: A renaissance for SRC. *Nat Rev Cancer* 2004;4:470–480.
- 62 Jain S, Wang X, Chang CC, Ibarra-Drendall C, Wang H, Zhang Q, et al.: Src Inhibition Blocks c-Myc Translation and Glucose Metabolism to Prevent the Development of Breast Cancer. *Cancer Res* 2015;75:4863–4875.
- 63 Pal R, Palmieri M, Chaudhury A, Klisch TJ, di Ronza A, Neilson JR, et al.: Src regulates amino acid-mediated mTORC1 activation by disrupting GATOR1-Rag GTPase interaction. *Nat Commun* 2018;9:4351.
- 64 Tillander V, Arvidsson Nordström E, Reilly J, Strozyk M, Van Veldhoven PP, Hunt MC, et al.: Acyl-CoA thioesterase 9 (ACOT9) in mouse may provide a novel link between fatty acid and amino acid metabolism in mitochondria. *Cell Mol Life Sci* 2014;71:933–948.
- 65 Bastie CC, Zong H, Xu J, Busa B, Judex S, Kurland IJ, et al.: Integrative Metabolic Regulation of Peripheral Tissue Fatty Acid Oxidation by the Src Kinase Family Member Fyn. *Cell Metabolism* 2007;5:371–381.
- 66 Alexson SEH, Svensson LT, Nedergaard J: NADH-sensitive propionyl-CoA hydrolase in brown-adipose-tissue mitochondria of the rat. *Biochim Biophys Acta* 1989;1005:13–19.
- 67 Park JH, Vithayathil S, Kumar S, Sung P-L, Dobrolecki LE, Putluri V, et al.: Fatty Acid Oxidation-Driven Src Links Mitochondrial Energy Reprogramming and Oncogenic Properties in Triple-Negative Breast Cancer. *Cell Rep* 2016;14:2154–2165.
- 68 Tarabra E, An Lee T-W, Zammit VA, Vatish M, Yamada E, Pessin JE, et al.: Differential activation of Fyn kinase distinguishes saturated and unsaturated fats in mouse macrophages. *Oncotarget* 2017;8:86634–86645.
- 69 Spriet LL, Tunstall RJ, Watt MJ, Mehan KA, Hargreaves M, Cameron-Smith D: Pyruvate dehydrogenase activation and kinase expression in human skeletal muscle during fasting. *J Appl Physiol* 2004;96:2082–2087.